Investigation of strain effect on the hole mobility in GOI tri-gate pFETs including quantum confinement

Qin Jie-Yu(秦洁宇)[a)b)], Du Gang(杜 刚)[b)], and Liu Xiao-Yan(刘晓彦)[b)†]

[a)] *Shenzhen Graduate School, Peking University, Shenzhen* 518055, *China*
[b)] *Institute of Microelectronics, Peking University, Beijing* 100871, *China*

(Received 21 March 2014; revised manuscript received 29 April 2014; published online 10 August 2014)

The strain impact on hole mobility in the GOI tri-gate pFETs is investigated by simulating the strained Ge with quantum confinement from band structure to electro-static distribution as well as the effective mobility. Lattice mismatch strain induced by HfO_2 warps and reshapes the valence subbands, and reduces the hole effective masses. The maximum value of hole density is observed near the top corners of the channel. The hole density is decreased by the lattice mismatch strain. The phonon scattering rate is degraded by strain, which results in higher hole mobility.

Keywords: strain, quantum effect, tri-gate, GOI

PACS: 85.30.Tv, 73.63.Nm, 73.50.Bk, 46.25.−y **DOI:** 10.1088/1674-1056/23/10/108501

1. Introduction

The continuous downscaling of the planar metal–oxide–semiconductor field-effect transistor (MOSFET) has boosted the performance of the transistor over the last decades. Due to the short channel effects (SCEs), it is difficult to scale the gate length of the planar MOSFET down to sub-20 nm. Various multi-gate MOSFETs, such as FinFET and tri-gate MOSFET, are proposed as substitution architectures of the planar MOSFET for the excellent immunity to performance variation and short channel effects.[1–3] Germanium with high intrinsic mobility is used as one of the alternative channel materials.[4,5] Previous work indicates that strain, such as mechanical stress and lattice mismatch strain, is induced into the channel due to the integration of strain engineering, which will modify the electronic structure of the semiconductor and influence the carrier transport characteristics of the device.[6,7] However, few works investigate the effective mobility in Ge non-planar MOFETs with strain and quantum confinement at the same time.

In this work, we calculate the strain distribution and the valence subband structure of the GOI tri-gate pFETs surrounded by high-k dielectric (HfO_2). The quantum-confined hole density distribution in both strained and unstrained devices are also compared. Finally, the effective hole mobility is investigated.

2. Simulation method and device structure

The schematic cross section of the tri-gate GOI p-channel metal–oxide semiconductor (PMOS) is shown in Fig. 1. The height and the width of the germanium channel are both 10 nm, and the thickness of the high-k gate dielectric is 2 nm. The origin of the x–y plane is located at the center of the channel. The strain distribution induced by HfO_2 is computed by the continuum elastic model.[8–10] The valence band structure is calculated by the 6×6 $\boldsymbol{k}\cdot\boldsymbol{p}$ method, in which the strain is included as a perturbation Hamiltonian.[11–13] The two-dimensional Poisson–Schrödinger[14,15] self-consistent solver is developed to evaluate the confinement of the tri-gate on the hole density distribution on the transverse plane. The Schrödinger equation and the Poisson equation are expressed as:

$$\left[-\frac{\hbar^2}{2m^*}\nabla^2+U(x,y)\right]\psi(x,y)=E\psi(x,y), \tag{1}$$

$$\nabla\left[\varepsilon_{\mathrm{r}}\nabla U(x,y)\right]=-\frac{q^2}{\varepsilon_0}\left[p(x,y)-p_0\right], \tag{2}$$

where m^* is the hole effective mass and $\psi(x,y)$ is the wave function of eigenenergy E. ε_{r} is the relative dielectric permittivity of Ge and HfO_2. $p(x,y)$ and $U(x,y)$ are the hole density distribution and potential distribution, and

$$p(x,y)=\sum_i|\psi_i(x,y)|^2\int_{E_i}^{+\infty}f(E-E_F)\,g(E)\,\mathrm{d}E.$$

With the two-dimensional (2D) Poisson–Schrödinger self-consistent solver, we can calculate the potential and hole density distributions in the tri-gate GOI pFETs with quantum confinement. The strain impact on the hole density distribution can be included through the hole effective mass (m^*) in Eq. (1), which can be extracted from the valence band structure.

The acoustic-phonon-limited hole mobility and the optical-phonon-limited hole mobility are calculated using the Kubo–Greenwood formula.[16,17] The acoustic phonon scattering rate and the optical phonon scattering rate are expressed

†Corresponding author. E-mail: xyliu@ime.pku.edu.cn

© 2014 Chinese Physical Society and IOP Publishing Ltd

as:

$$\left(\frac{1}{\tau_{\rm ac}}\right)^{ii'} = \frac{4\pi\Sigma_{\rm d}^2 kT}{\rho\hbar^2 u^2} g_{\rm 1D}^{i'}(E) F^{ii'}, \quad (3)$$

$$\left(\frac{1}{\tau_{\rm op}}\right)^{ii'} = \frac{2\pi D_{\rm op}^2}{\rho\omega_\gamma} g_{\rm 1D}^{i'}\left(E \pm \hbar\omega_\gamma\right) \frac{1 - f\left(E \pm \hbar\omega_\gamma\right)}{1 - f(E)} \times \left(n_{\rm ph} + \frac{1}{2} \mp \frac{1}{2}\right) F^{ii'}, \quad (4)$$

where $\tau_{\rm ac}(E)$ and $\tau_{\rm op}(E)$ are the momentum relaxation times for acoustic phonon scattering and optical phonon scattering, respectively. $\Sigma_{\rm d}$ is the acoustic deformation potential, $D_{\rm op}$ is the optical deformation potential, and $\hbar\omega_\gamma$ is the optical phonon energy. The parameters for scattering in Ge are employed from Ref. [18].

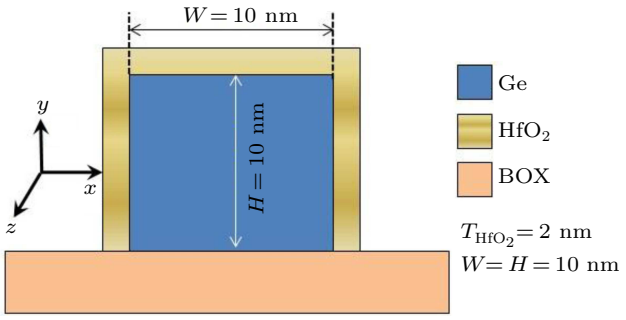


Fig. 1. (color online) The Cross-sectional view of tri-gate GOI PFET.

3. Results and discussion

3.1. Strain distribution and valence band structure

The principle strain distributions along the x axis (ε_{xx}), y axis (ε_{yy}), and z axis (ε_{zz}) in the strained GOI tri-gate pFET are shown in Fig. 2. The lattice constant of HfO_2 is 0.5116 nm, which is smaller than that of germanium (0.5646 nm). Thus, the principle strain ε_{zz} is compressive (-0.06278) in the channel. ε_{xx} is tensile near the BOX and compressive near the top of the channel. However, ε_{yy} is compressive near the BOX and tensile near the top of the channel.

The valence band structures of the simulated devices are revealed in Fig. 3. In the unstrained device, the maximum energy of the valence band is -27.29 meV. The hole effective masses of the three top-most subbands are $0.043m_0$, $0.085m_0$, and $0.068m_0$ respectively. As shown in Fig. 3(b), the lattice mismatch strain warps the valence subbbands more parabolic, and moves the bands up, which leads to higher maximum energy. The hole effective masses of the first, second, and third subbands are $0.038m_0$, $0.047m_0$, and $0.047m_0$, which are lighter than those of the unstrained GOI tri-gate pFETs.

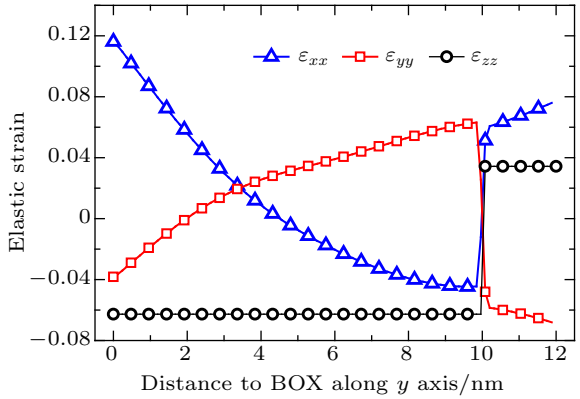


Fig. 2. (color online) The strain tensor component distribution along the y axis ($x = 0$).

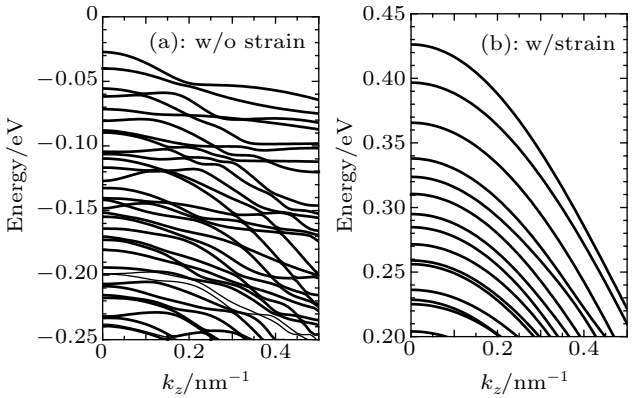


Fig. 3. The valence band structure of different GOI tri-gate pFETs. (a): w/o strain effect; (b): with strain effect.

3.2. The hole density distribution

Based on the 2D Poisson–Schrödinger self-consistent solver, the hole density distribution and the potential distribution in the GOI tri-gate pFETs under different gate biases are calculated. Figure 4 plots the quantum-confined hole density distribution along the y axis ($x = 0$) in the unstrained GOI tri-gate pFET with -1.0-V gate bias, and the classical hole density is also presented. Compared with the classical case, the position of the highest hole density moves to the center area of the channel, and more holes distribute near the center area of the channel due to the quantum effects. When the gate

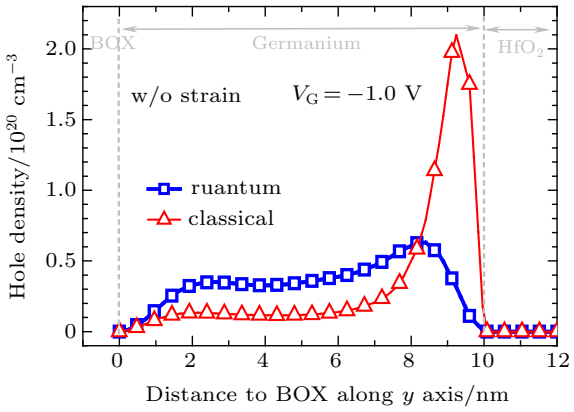


Fig. 4. (color online) The classical and quantum-confined hole density distribution along the y axis ($x = 0$) in the unstrained GOI tri-gate pFET ($V_{\rm G} = -1.0$ V).

bias is −1.0 V, the inversion hole density of the classical case is 1.22×10^8 cm^{-1}, and that of the quantum-confined case is only 4.22×10^7 cm^{-1}, which is 65.4% lower than the previous one.

Figures 5(a) and 5(b) plot the hole density distribution at −1.0-V gate voltage in the unstrained and strained devices respectively. As shown in Fig. 5, the hole density distribution is axially-symmetrical in both unstrained and strained devices, and the axis of symmetry is the y axis ($x = 0$). Higher hole density distribution is observed at the top corners and bottom corners of the channel. In the unstrained GOI tri-gate pFET, the highest value of hole density near the top corners is 8.94×10^{19} cm^{-3}. However, the highest value of hole density near the bottom corners is 6.63×10^{19} cm^{-3}, which is lower than that of the top corners. Similar hole density distribution is also observed in the strained device. The maximum hole density near the top corners and the bottom corners are 4.48×10^{19} cm^{-3} and 3.92×10^{19} cm^{-3}, which are lower than those in the unstrained device.

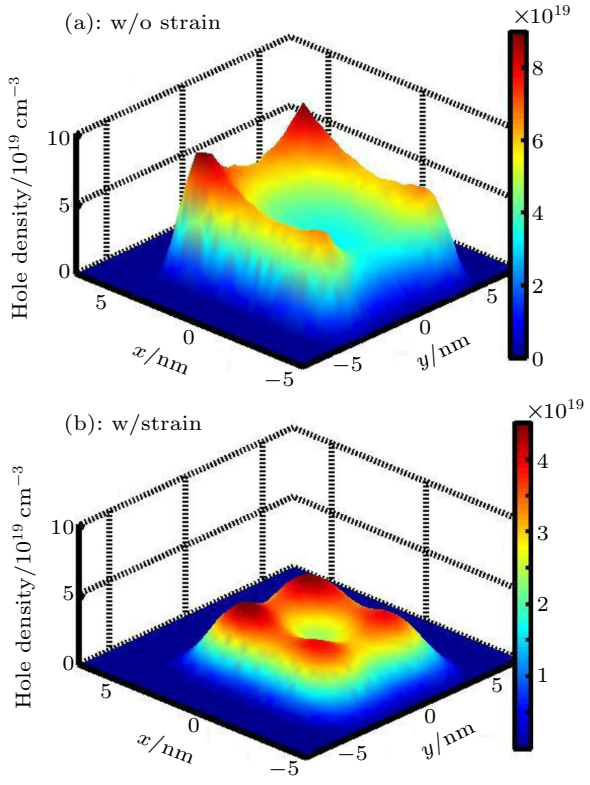


Fig. 5. (color online) The hole density distribution in the GOI tri-gate pFETs ($V_G = -1.0$ V), (a): w/o strain; (b): with strain.

Figures 6(a) and 6(b) show the hole density distribution along the y axis ($x = 0$) in the GOI tri-gate pFETs. At low gate bias, the holes mainly distribute near the center of the Ge channel in both strained and unstrained devices. The hole density increases with increasing gate bias, and most of the hole distributes near the top area of the channel at higher gate bias. The maximum of the hole density is observed in the top area of the channel. When the gate bias is −1.0 V, the maximum hole density in the unstrained device is 6.30×10^{19} cm^{-3} as revealed in Fig. 6(a), and the distance between the position of the

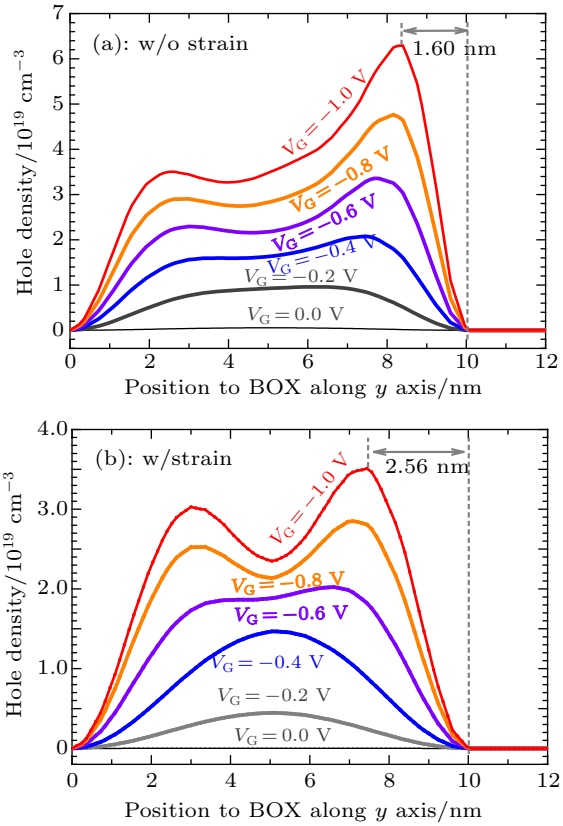


Fig. 6. (color online) The hole density distribution along the y axis ($x = 0$), (a): w/o strain; (b): with strain.

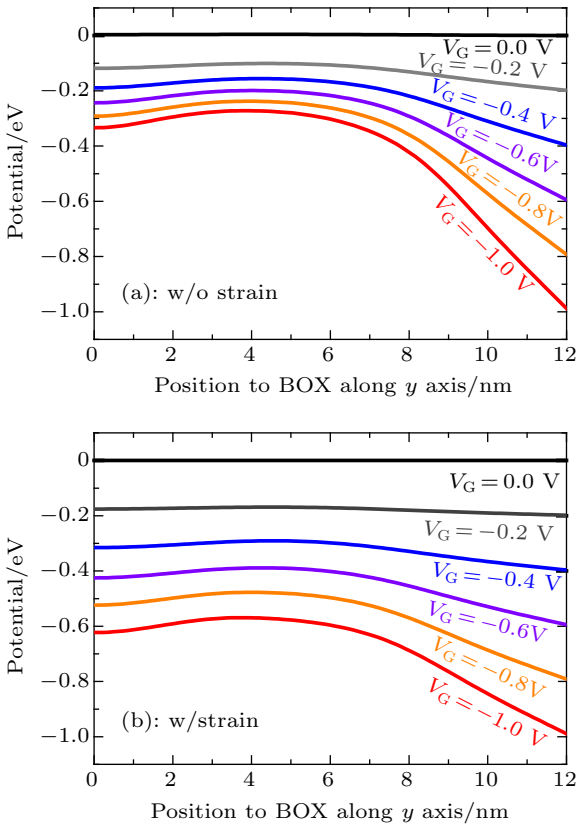


Fig. 7. (color online) The potential distribution along the y axis ($x = 0$), (a): w/o strain; (b): with strain.

maximum hole density to the Ge–HfO_2 interface is 1.60 nm. However, those values of the strained device are 3.51×10^{19} cm^{-3} and 2.56 nm respectively. The inversion hole density in the strained GOI tri-gate pFET is only 1.94×10^7 cm^{-1}. Figures 6(a) and 6(b) reveal that the lattice mismatch strain induced by the HfO_2 lowers the hole density in the GOI tri-gate pFETs. It is because the DOS (density of states) is directly proportional to the square root of the effective mass. Compared with the unstrained GOI tri-gate pFET, the lighter hole effective masses of the strained device lead to lower inversion hole density. Figures 7(a) and 7(b) show the potential distribution along the y axis ($x = 0$) in the GOI tri-gate pFETs. The barrier increases with increasing gate bias, and the barrier of the unstrained device is higher than that of the strained device with the same gate voltage.

3.3. Hole effective mobility

Figure 8(a) illustrates the hole effective mobility in the strained and unstrained GOI tri-gate pFETs under different effective electric fields, both acoustic phonon scattering and optical phonon scattering are considered. The hole mobility decreases with increasing effective electric fields, and the hole mobility is boosted by strain induced by HfO_2. When the effective electric field is 0.2 MV/cm, the hole mobility in the unstrained device is 80.68 $cm^2 \cdot V^{-1} \cdot s^{-1}$, and the hole mobility in the strained device is 175.08 $cm^2 \cdot V^{-1} \cdot s^{-1}$, which is 2.2 times as high as the previous one. When the effective electric field is 0.8 MV/cm, the hole mobility in the unstrained device is 53.22 $cm^2 \cdot V^{-1} \cdot s^{-1}$, and the hole mobility in the strained device is 88.30 $cm^2 \cdot V^{-1} \cdot s^{-1}$, which is 65.9% higher than the previous one. The hole scattering rate with −1.0-V gate voltage is shown in Fig. 8(b). A larger hole scattering rate is observed in the unstrained device, which will lead to smaller hole mobility. Table 1 summarizes the product of hole effective mobility and inversion hole density ($\mu \cdot p$) in both strained and unstrained GOI tri-gate pFETs. Higher $\mu \cdot p$ is observed in the strained device, which will lead to boosted drain current.

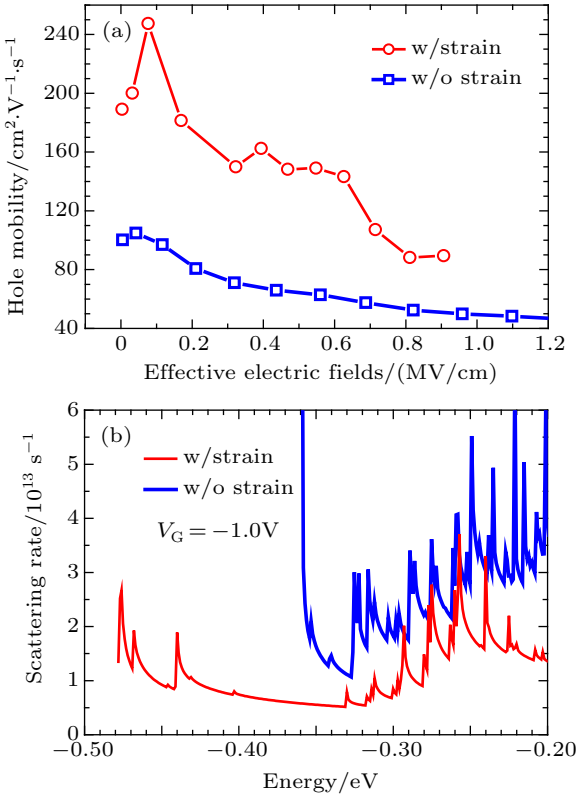


Fig. 8. (color online) The hole mobility versus the effective electric field (a), and the hole scattering rate with −1.0-V gate voltage (b).

Table 1. The product of hole effective mobility and inversion hole density in different GOI tri-gate pFETs. (Unit: $cm \cdot V^{-1} \cdot s^{-1}$).

Gate voltage/V	Type	
	Unstrained	Strained
−0.5	1.02×10^9	1.08×10^9
−1.0	2.04×10^9	2.90×10^9

4. Conclusions

The effect of lattice mismatch strain on the hole transport characteristics in the GOI tri-gate pFETs is investigated including the quantum effect. Compressive strain induced by HfO_2 moves the valence subbands up, warps the band more parabolically, and leads to lighter hole effective masses. The maximum value of hole density is observed near the top corners of the channel. The strain degrades the potential of the channel and results in less hole density in the strained device. The lattice mismatch strain also decreases the phonon scattering rate and increases the hole mobility of the GOI tri-gate MOSFET.

References

[1] Auth C 2012 *IEEE Custom Interrgrated Circuits Conference*, September 9–12, 2012, San Jose, CA, USA

[2] Kuhn K J 2012 *IEEE Trans. Electron Dev.* **59** 1813

[3] Zhang S M, Shi J W, Liu M D, Li J, Guo S X and Wang W 2004 *Chin. Phys. Lett.* **21** 164

[4] Lee M L, Fitzgerald E A, Bulsara M T, Currie M T and Lochtefeld A 2005 *J. Appl. Phys.* **97** 011101

[5] Ao J P, Zeng Q M, Zhao Y L, Li X J, Liu W J, Liu S Y and Liang C G 2000 *Chin. Phys. Lett.* **17** 619

[6] Qin J Y, Liu X Y and Du G 2013 *Chin. Phys. B* **22** 107104

[7] Qin J Y, Zhang J J, Du G, Zhang X and Liu X Y 2012 *IEEE International Conference on Solid-State and Integrated Circuit Technology*, October 29–November 1, 2012, Xi'an, China

[8] Sondergaard N, He Y, Fan C, Han R Q, Guhr T and Xu H Q 2009 *J. Vac. Sci. Technol. B* **27** 827

[9] Liu Y M, Yu Z Y and Ren X M 2009 *Chin. Phys. B* **18** 16

[10] Xu H H, Liu X Y, He Y H, Fan C, Du G, Sun A D, Han R Q and Kang J F 2010 *Chin. Phys. B* **19** 014601

[11] Bahder T 1990 *Phys. Rev. B* **41** 11992

[12] Kane E O 1956 *J. Phys. Chem. Solids* **1** 82

[13] He Y H, Zhao Y N, Fan C, Liu X Y and Han R Q 2009 *Front. Electr. Electron. Eng. China* **4** 342

[14] Colinge J P 2007 *Solid-State Electron.* **51** 1153

[15] Fischetti M V, Ren Z, Solomon P M, Yang M and Rim K 2003 *J. Appl. Phys.* **94** 1079

[16] Kotlyar R, Obradovic B, Matagne P, Stettler M and Giles M D 2004 *Appl. Phys. Lett.* **84** 5270

[17] Fischetti M V and Laux S E 1996 *J. Appl. Phys.* **80** 2234

[18] Zhang Y, Fischetti M V, Soree B, Magnus W, Heyns M and Meuris M 2009 *J. Appl. Phys.* **106** 083704